Toxicology of the Nose and Upper Airways

Edited by

John B. Morris
University of Connecticut
Storrs, Connecticut, U.S.A.

Dennis J. Shusterman
University of California
San Francisco, California, U.S.A.

2010

informa
healthcare

New York London

6 Upper Airway Dosimetry of Gases, Vapors, and Particulate Matter in Rodents

John B. Morris

Department of Pharmaceutical Sciences, School of Pharmacy, University of Connecticut, Storrs, Connecticut, U.S.A.

Bahman Asgharian

Applied Research Associates, Raleigh, North Carolina, U.S.A.

Julia S. Kimbell

Otolaryngology/Head and Neck Surgery, University of North Carolina, Research Triangle Park, North Carolina, U.S.A.

INTRODUCTION

The nasal cavity is an extremely common site of injury following inhalation exposure in rodents. The significance of nasal lesions in rodents relative to the potential risk to humans is often poorly understood. Experience has indicated that the relationships between airborne concentration and delivered dose to nasal tissues are often critical to the interpretation of animal toxicity data. This is not surprising given that dose–response is one of the most fundamental principles of toxicology. From this perspective, an understanding of the delivered dose relationships of an inhaled material is fundamental to assessment of its hazard. It is these relationships that are the focus of the current chapter.

Nasal dosimetry is the term used to describe the relationships between airborne concentration and the dose of inhaled material delivered to nasal target sites. Nasal dosimetric relationships are complex and species-specific. For this reason, useful interpretation and extrapolation of laboratory animal inhalation toxicity data can be difficult. For inhaled materials, the site selectivity of damage is due to regional toxicokinetic (delivered dose) and/or toxicodynamic (tissue sensitivity) properties of the toxicant and airways. While the focus of this chapter is on nasal dosimetry, it is essential to recognize that nasal responses in the rodent may be sentinels for potential lower airway injury in humans simply because of toxicokinetic (delivered dose) issues. Thus, nasal rodent toxicity data are best interpreted in a much broader sense than merely being reflective of risk to nasal tissues alone in man.

The inhalation toxicity of hydrofluoric acid vapor provides a useful example of the importance of this phenomenon. Rodents are obligate nose breathers, whereas humans are capable of mouth breathing. Indeed, it has been estimated that as much as 40% of the population respires, at least in part, through their mouth (1). Acute inhalation exposure of rats to hydrofluoric acid vapor results in nasal injury with no damage in the lower airways (2,3). It has been estimated that greater than 99.7% of inspired hydrofluoric acid vapor is scrubbed from

the airstream in the upper respiratory tract of the rat with less than 0.3% penetrating to the lower airways, providing a toxicokinetic (delivered dose) basis for its regional toxicity (4). If rats are forced to breathe through their mouth via insertion of an oropharyngeal cannula, acute hydrofluoric acid vapor exposure results in tracheobronchial rather than nasal injury. This elegantly simple experiment demonstrates the importance of inhalation dosimetry in determining the site of injury (3). In humans, lower airway injury results from hydrofluoric acid exposure (e.g., 5) indicating, at least for this irritant, that nasal injury in the rodent was indeed predictive of lower airway risk in man. The columnar mucociliated epithelium of the nasal passages is structurally similar to that of the large lower airways (chap. 2) suggesting the sensitivity of these tissues might be similar. Little information is available in this regard; however, recent studies suggest the nasal and tracheal epithelium are equally responsive to the irritant 2,3-butanedione (6). While the relationship of nasal versus tracheobronchial tissue sensitivity is an area in need of much research, it is nonetheless clear that nasal injury in rodents may be predictive of lower airway risk in mouth-breathing humans.

The goal of this chapter is to highlight the basic principles and the current state-of-the-art relative to the nasal dosimetry of inspired gases, vapor, and particles. Since the physical factors that control dosimetry of gases and vapors differ from those controlling particle dosimetry, they are discussed separately. Both experimental and computational approaches to define dosimetric relationships are discussed. Perhaps not surprisingly, both approaches lead to similar predictions. The strengths, weaknesses, and potential usefulness of these approaches are highlighted along with the integration of experimental and computational data.

DOSIMETRY OF GASES AND VAPORS

Basic Principles

The ability of the upper respiratory tract to scrub gases and vapors from the airstream has long been appreciated (7). The absorption of gas or vapor molecules into airway mucosa is a dynamic reversible process in which gas molecules may be absorbed (typically during inspiration) and desorbed (typically during expiration). It is the balance between these processes that determines the net transfer of gas molecules to airway tissues. Various terms have been used to describe this phenomenon in living animals including: nasal uptake, nasal extraction, nasal deposition, and nasal scrubbing. In the most simplistic sense, the volume and/or flow rate of air and the mass of nasal tissues will be important factors relative to nasal uptake. The nose of the rodent is not uniformly ventilated, with differing regions of the nose receiving widely differing fractions of the inspired air (8,9). Thus, it can be appreciated that the deposition patterns and tissue doses will differ regionally throughout the nose.

There have been a number of publications in recent years describing the basic principles of gas and vapor uptake in the respiratory tract (e.g., 10–12). Chemical engineering principles in particular provide useful insights (10,13). The uptake process consists of three steps: convection and diffusion of airborne gas or vapor molecules to the air:tissue interface, transfer across that interface, and diffusion of tissue-borne gas or vapor away from the interface. From the

engineering perspective, these steps can be quantified on the basis of air:phase, tissue:phase, and overall mass transfer coefficients (13,14). These coefficients relate to the speed and efficiency of each of these processes. The use of these coefficients is discussed below.

A fundamental physicochemical principle governing gas or vapor uptake is Henry's Law, which states that the concentration (or partial pressure) of gas or vapor in a liquid phase at equilibrium is directly proportional to the concentration (or partial pressure) in the gas phase above that liquid. Conceptually, this means that airway tissues have the potential to become saturated with gas or vapor molecule. The proportionality constant can be expressed in many ways, but the most common approach is via a tissue:air partition coefficient, which is reflective of the ratio of the concentration at equilibrium of gas or vapor in tissue divided by that in air.

The importance of tissue solubility in influencing regional uptake of vapors has long been realized and was perhaps first discussed from a theoretical and pragmatic perspective nearly a century ago by Haggard (15). *It is absolutely essential, however, to realize that this concept holds only for parent gas or vapor molecules.* If the gas or vapor is converted to another chemical species, either by direct chemical reaction or metabolism, then direct application of Henry's Law is inappropriate. Some vapors are so highly reactive that they are instantly removed from tissue. In such circumstances, tissue concentrations are negligible and the tissue acts as an infinite sink. Tissue factors are often unimportant in such cases and vapor or gas uptake is "air-driven" and is critically dependent only on air-phase phenomenon. Formaldehyde offers an example of such a case (16). The US EPA terms these gases "category 1" gases (13). For all other gases or vapors, the concentration of vapor in tissue (e.g., "backpressure") will influence and/or control the uptake process. As discussed below, differing theoretical modeling approaches are typically used for these two types of gases or vapors. Nasal vapor uptake efficiency can range from essentially 0% for low solubility (low partition coefficient) vapors or gases to essentially 100% for highly soluble, highly reactive vapors or gases.

For gases or vapors for which tissue backpressure influences uptake, it is important to understand the tissue factors that are involved. In essence, tissue clearance pathways serve to reduce the concentration of vapor in tissue and will enhance the uptake process as additional vapor or gas molecules will be transferred to tissue to maintain Henry's Law equilibrium (provided there is sufficient time). Experimentally, a steady state occurs in which the uptake rate equals the tissue clearance rate. Removal of vapor via the bloodstream is one such clearance pathway. In fact, the use of vapor uptake rates to measure airway perfusion rates is not new (103). Biotransformation enzymes are highly expressed in nasal tissue (chap. 5), metabolic clearance represents another important clearance pathway. Direct reaction is the third common pathway for removal of parent vapor molecules from airway tissues.

In summary, gas or vapor uptake is a dynamic process in nasal tissues that is dependent upon the gas or vapor solubility as measured by the tissue:air partition coefficient, the rate at which vapor directly reacts with tissue substrates and the rate at which vapor is metabolized by biotransformation pathways and the airway perfusion rate. As exposures progress these clearance pathways can change. For example, substrates for reaction (e.g., glutathione for electrophilic

vapors) can become depleted altering uptake efficiencies (17). Physiological factors (e.g., nasal vasodilation) can occur (98,100). Uptake should not be viewed as static but as a process that can change quickly as biochemical and/or physiological conditions in the nose change.

Experimental Dosimetry Data

Since nasal tissues of laboratory animals are easily accessible, measurements of nasal vapor uptake efficiencies date back nearly 50 years (18). Typically, an endotracheal tube is inserted in an anterior direction and vapor-laden air is drawn through the nose either under unidirectional or cyclic conditions. Measurement of vapor concentration in air entering the nose versus that in the endotracheal tube itself provides an estimate of uptake efficiency. An advantage of this approach is that definitive measures of uptake efficiency under defined airflow conditions are possible. A disadvantage is that it relies upon nonphysiological flow conditions in anesthetized animals.

A rich database exists on nasal uptake efficiency of gases and vapors, many of these data have been generated in the laboratory of one of the authors (JBM). Data are available on such diverse agents as the inorganic gases ozone (19), sulfur dioxide (20), nitrogen dioxide, inorganic and organic acids (4,17,21), the solvents ethanol, acetone and styrene (22,23,99), esters (24), and the reactive volatile organics acrolein (17,25,96), propylene oxide (26,27) and formaldehyde (28,29). Data are available on numerous species including the dog (20), rabbit (30), guinea pig, rat, hamster, and mouse (91,92,94,97). Experimental data obtained using physiological inspiratory flow rates in rats indicate low (10% or less) uptake efficiencies for low partition coefficient (blood:air partition coefficient <50), nonreactive, slowly metabolized vapors, to extremely high (>90%) for water-soluble highly reactive vapors (e.g., sulfur dioxide, chlorine, formaldehyde, ionizable acids). Intermediate uptake efficiencies are observed for vapors of intermediate partition coefficient (50–2000) that are slowly reactive and/or slowly metabolized.

As noted above, metabolism within nasal tissues serves to lower tissue concentrations and, therefore, enhances vapor uptake. A biological approach to confirm this phenomenon is to measure nasal uptake efficiency in control and metabolically inhibited animals. Stott and McKenna (31) were perhaps the first to document this phenomena by showing that the carboxylesterase inhibitor TOCP diminished nasal uptake efficiency of inspired ethyl acetate. This phenomenon has been studied extensively by Morris, who has showed via use of metabolic inhibitors that several biotransformation enzymes including carboxylesterase (93), alcohol dehydrogenase (95), aldehyde dehydrogenase (91), and cytochrome P450 mixed functions oxidases (23,95) can serve to enhance nasal scrubbing efficiency. It should be recognized that the toxicological importance of metabolism relates not only to its effect on nasal dosimetry but also on whether the biotransformation reflects an activation or detoxification pathway (chap. 5).

Other experimental dosimetry work has focused on the measurement of specific markers of dose called dosimeters in tissues. Direct measurement of local tissue dose is often difficult. However, dosimeters based on potential modes of action underlying tissues responses can be very useful both for understanding the biological basis for the response and for extrapolating dose–response relationships from animals to people. One example of such a dosimeter is found

in studies on DNA–protein crosslinks (DPX), which form in tissue exposed to formaldehyde gas (32). Correlation of high DPX levels with formaldehyde-induced lesion locations in rats and primates (33,34) led to the use of DPX to extrapolate animal data to people in subsequent human health risk assessment studies of formaldehyde gas (35,36).

Dosimetry Modeling

Three approaches have been used to model nasal gas and vapor uptake in experimental animals: the computational fluid dynamic (CFD) approach developed by Kimbell (9), the physiologically based pharmacokinetic (PBPK) approach developed by Morris (37), and the hybrid CFD–PBPK approach, an insightful contribution first proposed by Frederick (38,39). The hybrid model represented a significant advance and provided a PBPK-based modeling approach superior to that first proposed by Morris et al. (37). The three modeling approaches are all theoretically and experimentally valid. They have differing strengths and weaknesses; selection of the most appropriate approach is dependent on the physical chemical properties of the gas or vapor of interest and how much anatomical detail is needed in modeling outcomes.

The development of the CFD modeling approach was based on observations of the site specificity of formaldehyde-induced nasal tumors in rats. These tumors invariably appeared in selected regions of the nose, leading Morgan et al. (40) to hypothesize that high delivery of formaldehyde to these regions (e.g., hotspots) occurred. Since formaldehyde is highly soluble and reactive, nasal tissue likely represents an infinite sink; therefore, this phenomena must be reflective of factors occurring in the air phase. To examine this possibility, streamlines were first assessed in nasal casts. These studies suggested a concordance between major streams of inspired air and lesion locations in both rats and primates (41) but did not provide local dose estimates.

The level of anatomical detail available in nasal lesion data drove the concurrent development of three-dimensional (3D) anatomically accurate dose prediction models for inhaled gases in the nasal passages of rats, rhesus monkeys, and a number of humans (8,9,42–46). These models use a CFD approach to predict inhaled gas flux from nasal airspaces to airway walls. The CFD models have been used to study mechanisms of toxicity for ozone (47,48), formaldehyde (9,36,41,49–52), hydrogen sulfide (53–55), and acrolein (56) and to support risk assessment activities for formaldehyde (28,29,35,57–60), acidic vapors (38), methyl methacrylate (61), acrylic acid (62), and esters (39).

The CFD studies revealed that the nasal passages are not uniformly ventilated. For example, only ~12% of the inhaled airstream in the rat passes over a dorsal medial pathway to the olfactory-lined ethmoturbinates. [Concurrently a similar estimate of olfactory mucosal airflow was independently obtained by a PBPK approach (37).] This knowledge, coupled with chemical engineering mass transfer principles, resulted in the first estimation of intranasal regional deposition patterns of an inspired vapor, formaldehyde (9). As shown in Figure 1, flux (mass of formaldehyde entering tissue per surface area) is not uniformly distributed throughout the nose but is localized in hotspots. The location of these hotspots associated closely with the location of formaldehyde-induced tumors (51), thus supporting the original hypothesis regarding the importance of localized delivery of formaldehyde within the nose.

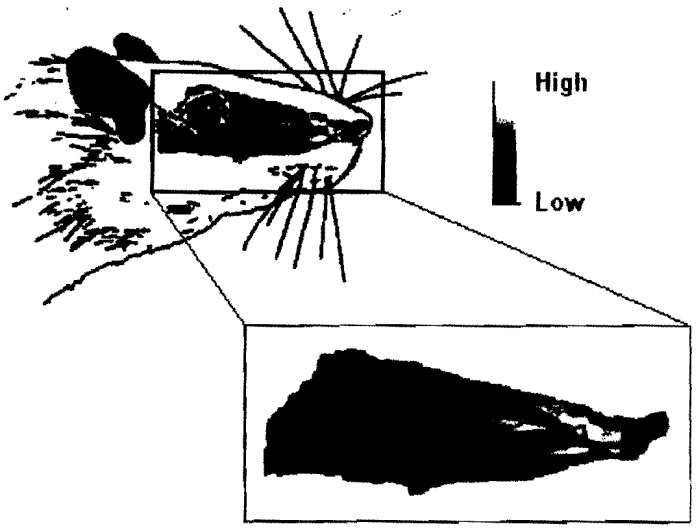

FIGURE 1 Lateral view of rat head showing nasal passages. Inset shows computational model of the nasal passages shaded by flux (rate of gas uptake from air to tissue surface at the tissue surface).

The success of the CFD approach has led to its use to model other vapors including hydrogen sulfide and acrolein. For both agents, a close association between lesion location and flux was observed (54,56). A strong advantage of this approach is that it provides a means of estimating delivered dosage rates at specific regions within the nose as well as providing a means of examining the effect of anatomic changes on delivered dosage rates. This approach has been extended to the human nose to extrapolate animal toxicity data to the humans, not on the basis of inspired concentration, but on the basis of regional flux to precise locations within the nose (54). Another significant contribution of the CFD modeling effort is that it provides estimates of gas-phase mass transfer coefficients. These coefficients are essential components of the current CFD–PBPK models. A disadvantage of the CFD approach is that it is not easy to carry out automated optimizations of fitted model parameters for tissue uptake; previous studies have used a combined CFD–PBPK approach to conduct optimizations (55).

PBPK models provide an approach in which to explicitly incorporate physiologically and biologically constrained data into a dosimetry model. The first PBPK nasal dosimetry model was developed by Morris et al. (37). In this approach, air is allowed to pass over tissue, which is modeled as stacks of 10-μm thick mucus, epithelial and submucosal compartments. Blood perfuses the submucosal compartments and vapor transfer between compartments occurs on the basis of tissue diffusivity. The overall depth of the tissue layers is based on anatomical measurements. Tissue metabolism rates, based on in vitro measurements, can be assigned independently to respiratory or olfactory mucosa and, within each mucosal type, separately to epithelial or submucosal compartments. In this first modeling effort, uptake data from a variety of vapors were fit to provide estimates of nasal perfusion rate and air flow patterns within the nose. The best fit estimated that 8% of the inspired air penetrates over the olfactory epithelium, a value similar to that obtained independently in Ref. 10.

A significant disadvantage of the PBPK model approach is that it did not explicitly incorporate air phase diffusion/mass transfer phenomena. Frederick et al. (38) provided a mechanism to incorporate these phenomena into the model structure with the hybrid CFD–PBPK model. In the hybrid model, vapor is allowed to enter (or desorb from) the mucus lining layer in accordance with an overall mass transfer coefficient. This is calculated on the basis of the air-phase mass transfer coefficient that is provided by the CFD models and a tissue phase mass transfer coefficient estimated from the tissue:air partition coefficient and the molecular diffusivity. With this approach, truly first principle models were developed for ethyl acrylate and acrylic acid (38,39), meaning that every parameter in the model was pre-assigned based on independent biological or physical measurement. Model output was then compared to experimental data and an extraordinarily close correspondence was seen. This approach has been successfully extended to a variety of vapors (6,63–65) and to describe uptake in the human (66).

Thus, the combined CFD–PBPK modeling efforts reported in the literature have taken one of two forms. In one form, enough information was available to calibrate the CFD model for the specific gas. Gas-specific flux estimates made by the CFD models were then handed off to PBPK models that estimated tissue dose (36,50,67). In the other form, the CFD models were used to calculate air-phase mass transfer coefficients, which depend only on air-phase diffusivity and airflow patterns. The coefficients are easily scalable to other air-phase diffusivities and can incorporate localized airflow effects when calculated regionally. Regional air-phase mass transfer coefficients derived from the rat and human nasal CFD models have been incorporated into PBPK models to estimate tissue dose when modeling goals do not require the complexity of the nasal CFD model (38,39,61,62).

The accuracy of inspiratory nasal airflow patterns predicted by rat, monkey, and human CFD models has been confirmed by comparison with experimental measurements (9,44,45). Confirmation of inhaled gas transport and uptake simulations using rat and monkey nasal CFD models has been demonstrated for formaldehyde (36,67) using formaldehyde-induced DNA–protein crosslinks measured in exposed F344 rats and rhesus monkeys (32–34).

The advantages of the CFD–PBPK modeling approaches are that it allows explicit incorporation of tissue-specific parameters into its structure. Since biotransformation enzymes are nonuniformly distributed between respiratory and olfactory mucosa (chap. 5), this is particularly important for vapors which are metabolized within the nose. A disadvantage of this approach is that it does not provide a means of estimating delivered dosage patterns within small regions of the nose (e.g., hotspots). Additionally, this modeling approach is ill suited to describe nasal dosimetry of highly soluble reactive gases and vapors because air-phase, not tissue-phase, factors control nasal uptake. Overall, it can be appreciated that the CFD and CFD–PBPK approaches are complimentary efforts, with the former being suited for localized dosimetry of water-soluble reactive vapors and the CFD–PBPK being suited for less soluble–less reactive vapors. Both approaches have been validated with experimental data, the needs of the study dictating the selection of modeling approach.

Integration of Experimental and Computational Approaches

Over the last 50 years, a rich database on nasal vapor and gas uptake has been developed. These data indicate that nasal vapor uptake can vary from essentially 0% to 100% depending on the properties of the gas or vapor. Critical vapor properties are solubility (tissue:air partition coefficient), and reactivity (either direct or enzymatically mediated). These data also provided critical quantitative insights into the factors which control the uptake process and ultimately to the development of mathematical models to describe uptake. The original modeling efforts were fit to uptake data to allow parameterization (8,37). These models have now become sufficiently advanced that they are developed a priori, with uptake measurements being made subsequently to validate the model-based predictions (e.g., 6,39). These models are extraordinarily useful as they facilitate extrapolation of data. For example, models that are validated with data obtained under nonphysiological flow conditions can be used to estimate uptake patterns during normal breathing and/or exercise. Such models can also be used to extrapolate nasal dosimetric relationships in animals exposed to high concentrations, to those in humans exposed to low concentrations. Delivered dose relationships are critical in determining the ultimate toxic response to inspired gases and vapors, thus dosimetric modeling is an essential aspect of evaluation and extrapolation of animal inhalation toxicity data.

DOSIMETRY OF PARTICLES

Basic Principles

Transfer of particles from the airstream to the tissue surface (termed deposition) is an irreversible process. Once deposited, insoluble particles can be removed by mechanical means including sneezing and mucociliary transport. Particles may also enter cells via dissolution and diffusion or by active (e.g., pinocytotic) pathways. These later processes are considered to constitute clearance mechanisms and are not considered herein. The fundamental processes determining transfer of particulates from a moving airstream to a tissue surface are well understood and include sedimentation, inertial impaction, and diffusion. Sedimentation is not thought to be important in the nose. Inertial impaction occurs due to the mass of the particle in motion, causing it to leave the airstream as the airstream bends. Inertial impaction increases with ρd^2 (particle density times particle diameter squared), and is important for fine and coarse particles (>0.5 μm in diameter). Diffusion (Brownian movement) results from the energy imparted by collisions of air molecules with particles and is related to $1/d$ (the inverse of the particle diameter) and is important for small particles (<0.1 μm). The diffusive process is particularly important for nanoparticles. Models for total respiratory tract particle dosimetry (e.g., ICRP) include explicit discussions of nasal particle deposition. Reviews are available summarizing data on regional particle deposition in animals and man (101,102).

Experimental Data

In Vivo Studies

Data from a limited number of experiments are available on measurements of aerosol deposition in the respiratory tracts of nonhuman primates and rats. A

recent study by Cheng et al. (68) reported measurements of head and lung deposition in anesthetized cynomolgus monkeys. The animals were exposed to 2.3- and 5.1-μm particles and head deposition fractions were found to be 39% and 58% for the two particle sizes. In rodents, inhalation exposures are conducted in nose-only chambers for which there is a good control over exposure concentration and delivery airflow rate. In addition, animal breathing parameters can be monitored accurately when animals are placed in a body plethysmograph. Particles can be sampled at one port of the nose-only tower for size analysis. Following the exposure, animals are sacrificed and dissected according to physiologically defined regions (head, tracheobronchial, pulmonary, etc.) and particle deposition is measured in each region.

Regional deposition of ultrafine particles have been reported by Chen et al. (69) for cigarette smoke particles, Wolff et al. (70) for aggregate 67Ga2O3 particles in Fischer-344 rats, and Dohlback and Eirefelt (71) and Dohlback et al. (72) for particle deposition in male Sprague-Dawley rats. Raabe et al. (73,74) measured deposition of fine and coarse particles in the head and lungs of Long-Evans rats. However, minute ventilations of the test animals were not measured and instead allometric equations were used for lung parameters. Therefore, uncertainty existed with the calculated deposition fractions. Asgharian et al. (75) repeated the study while the ventilation parameters were monitored throughout the exposure. Particle sizes ranged between 0.9 and 4.2 μm. Deposition for particles greater than 3 μm tended to decline, which may have been due to limitations with the inhalability of these particles.

Since the focus of inhalation exposure studies has primarily been on the measurements of lung deposition, limited data on head deposition have emerged from the above studies. Experiments to measure the deposition of particles in the nasal passages of rodents and nonhuman primates are scarce due to the difficulty and cost associated with conducting such experiments and also because it was not realized until very recently that the nasal airways serve as a potential route of transport of materials to the brain (76,77). Gerde et al. (78) devised a technique in which a catheter was inserted in the trachea distal to the nasal airways of anesthetized male Fischer 344 rats to allow measurements of ultrafine particle concentrations at the proximal and distal ends of the nasal region and calculate deposition fraction during steady inspiration and expiration. Quantification of particles in the airstream instead of on the nasal tissues eliminated uncertainty due to fast mucociliary clearance of deposited particles on the nasal surfaces. Measured deposition for particles between 5 nm and 100 nm at steady breathing rates of 200 mL/min to 600 mL/min was found to be similar to values measured in casts (79).

Kelly et al. (80) employed the same technique to measure deposition of fine and coarse aerosols in the nasal airways of female Long-Evans rats during steady and pulsatile breathing. Partial obstruction of the flow through the nasal airways due to the positioning of the catheter with respect to the head and possible leaks imposed a challenge to reliable and reproducible runs and may have contributed to variability in measurements. Deposition measurements were higher for pulsatile breathing than for steady breathing due to enhanced particle inertia at the peak flow. It was also observed that more particles were deposited during exhalation than during inhalation.

Studies in Nasal Molds

Difficulty with in vivo measurements has led investigators to build hollow molds of the nasal airways in which to conduct particle deposition experiments. Hollow molds have been created from nasal specimens, serial sections, and computer reconstructions using stereolithography techniques. The physical nasal molds can be used to measure particle deposition in situ, which can be used to confirm computer model (in silico) predictions. In addition, multiple runs may be made by varying the flow rate and particle size in the same setup and hence can collect more information in a short time when compared with in vivo measurements.

Kelly et al. (81) used a nasal mold to measure deposition fractions of 1–10 μm particles in the nasal passages of a 12-kg, male rhesus monkey for steady inspiration flow rates of 2–7 LPM. Particle deposition was described by a single inertial parameter that varied between 0% and 100% and showed a sigmoidal shape. Cheng et al. (79) measured pressure drop and deposition of ultrafine aerosol particles in a mold of the nasal passages of an adult male Fischer 344 rat. Measured nonlinear flow-pressure drop relationship indicated the presence of nonlaminar regimes in the flow. Measured depositions of 43 nm to 210 nm particles in the nasal mold were in agreement with in vivo measurements from inhalation studies (69,70,73).

Measurements of fine and coarse particle deposition, for which deposition in the nasal passages is by inertial impaction, are reported by Kelly et al. (82). Particles with sizes between 0.48 μm and 4.18 μm were passed through the nasal mold of a male 344 Fischer rat at flow rates of 100 to 900 mL/min for inspiratory and expiratory breathings. Collected data were in agreement with in vivo measurements and similar trends of deposition with flow type and direction were observed in in vivo measurements (80). Comparison of in vivo and in situ measurements suggested that good estimates of total nasal deposition in rats can be obtained by using nasal molds as surrogates for live animals (83).

Dosimetry Modeling

Empirical Studies

Losses of particles in the nasal airways are significant for two reasons. First, particles may deposit and accumulate locally and elicit toxicological response in the nasal airways or deposit and transport to the brain via the olfactory nerves. Second, to study toxicity of inhaled particles in the lung, one must determine the amount that passes through the nose and become available for deposition in the lung. Therefore, it is necessary to develop predictive models of particle deposition in the head based on the physics of airflow and particle transport. Consequently, models of particle deposition efficiency are sought as a function of parameters that control particle movement and deposition.

There are two main mechanisms that influence particle deposition in the nasal passages. Small particles are deposited by Brownian diffusion while fine and coarse particles are removed from the inhaled air by inertial impaction. A different mathematical model is required for each mechanism. Cheng et al. (79) postulated that due to nonlaminar characteristics of the flow, turbulent diffusion

was responsible for losses of ultrafine particles in the nasal passages and proposed the following relationship:

$$\eta = 1 - e^{\alpha D^{\beta} Q^{\gamma}} \tag{1}$$

where η is the deposition efficiency, D is the diffusion coefficient, and Q is the airflow rate through the nose, and α, β, and γ are fitted constants. Equation (1) exhibits increasing deposition efficiency with increasing diffusion parameter ($D^{\beta} Q^{\gamma}$) but decreasing efficiency with increasing particle size. Coefficients α, β, and γ were obtained by fitting equation (1) to deposition measurements made in a nasal mold (79). Additionally, Asgharian et al. (84) found by examining the governing equations of transport for the air and particles that deposition efficiency depends on D and Q, and proposed

$$\eta = \alpha D^{\beta} Q^{\gamma} \tag{2}$$

Similarly, coefficients α, β, and γ were found by fitting equation (2) to the measurements reported by Wong et al. (85).

Deposition efficiency by inertial impaction can be correlated with impaction parameter $d_{\alpha}^2 Q$, where d_{α} denotes particle aerodynamic diameter. Extending the mathematical model suggested by Rodulf et al. (86), Zhang and Yu (87) employed the following relationship to predict nasal deposition efficiency:

$$\eta = \left[\frac{(d_{\alpha}^2)^{\alpha}}{\beta + (d_{\alpha}^2)^{\alpha}} \right]^{\gamma} \tag{3}$$

Coefficients α, β, and γ were obtained by fitting equation (3) to the measurements by Raabe et al. (73,74) from a nose-only inhalation exposure conducted in Fischer 344 rats. The same model was employed by Kelly et al. (83) to predict nasal deposition efficiency in Long-Evans rats. Measured deposition fraction in live animals (80) and nasal mold (82) was used to find parameters α, β, and γ. Different models were obtained for inspiratory and expiratory steady and pulsatile breathings. Table 1 lists fitted parameters for equations 1–3 in different studies.

TABLE 1 Calculated Values of α, β, and γ Used in Equations 1–3

Reference	Experiment	Breathing	α	β	γ
(79)	Nasal mold	Inspiration, steady flow	−16.8	0.517	−0.234
		Expiration, steady flow	−14.0	0.517	−0.234
(84)	Nasal mold	Inspiration, steady flow	7.351	−0.2438	0.402
(87)	Nose-only inhalation	Normal	2.553	10^5	0.627
(83)	Nose-only inhalation	Inspiration, steady flow	2.42	10^5	0.27
		Expiration, steady flow	2.59	10^5	0.279
		Inspiration, pulsatile flow	2.88	10^5	0.304
		Expiration, pulsatile flow	3.26	10^5	0.262
(83)	Nasal mold	Inspiration, steady flow	3.00	10^5	0.907
		Expiration, steady flow	2.98	10^5	0.659
		Inspiration, pulsatile flow	3.78	10^5	0.539
		Expiration, pulsatile flow	3.88	10^5	0.447

The regional deposition of smaller particles, between 1 and 100 nm in diameter, has been studied in the rat nose computationally by Garcia et al. (88). In this study, estimates were developed of nanoparticle deposition in the nasal and, more specifically, olfactory regions of the rat. The rat CFD model of Kimbell et al. (8) was employed to simulate inhaled airflow and to calculate nasal deposition efficiency. Simulations predicted that olfactory deposition is maximum at 6–9% of inhaled material for 3–4 nm particles. The spatial distribution of deposited particles was predicted to change significantly with particle size, with 3-nm particles depositing mostly in the anterior nose, while 30-nm particles were more uniformly distributed throughout the nasal passages.

CONCLUSIONS

Dose–response is among the most fundamental principles of toxicology. This chapter has highlighted the current state of the art relative to nasal dosimetry of gases, vapors, and particles. Such evaluations are best performed in the context of risk to the entire respiratory tract, not merely risk to nasal tissues alone as inhaled materials can produce damage in the nasal passages, tracheobronchial tree, and/or the alveoli. Indeed, nasal damage in rodents may be the sentinel for lower airway risk in man. Regardless of the site of injury, delivered dosage rates are critically important in determining the toxic response to inhaled materials and, therefore, represent an essential aspect in inhalation risk assessment. With respect to nasal dosimetry, the physical/chemical factors influencing inhalation dosimetry are well understood and mathematic inhalation dosimetry models are sufficiently advanced to allow prediction of nasal dosimetry based on the physical/chemical properties of the gas, vapor, or particle of interest.

REFERENCES

1. DeSesso JM. The relevance to humans of animal models for inhalation studies of cancer in the nose and upper airways. Qual Assur 1993; 2:213–231.
2. Rosenholtz MJ, Carson TR, Weeks MH, et al. A toxicopathologic study in animals after brief single exposure to hydrogen fluoride. Am Ind Hyg Assoc J 1963; 24:253–261.
3. Stavert DM, Archuleta DC, Behr MJ, et al. Relative acute toxicities of hydrogen fluoride, hydrogen chloride and hydrogen bromide in nose- and pseudo-mouth-breathing rats. Fundam Appl Toxicol 1991; 16:636–655.
4. Morris JB, Smith FA. Regional deposition and absorption of inhaled hydrogen fluoride in the rat. Toxicol Appl Pharmacol 1982; 62:81–89.
5. Bennion JR, Franzblau A. Chemical pneumonitis following household exposure to hydrofluoric acid. Am J Ind Med 1997; 31:474–478.
6. Morris JB, Hubbs AF. Inhalation dosimetry of diacetyl and butyric acid, two components of butter flavoring vapors. Toxicol Sci 2009; 108:173–183.
7. Jordan EO, Carlson AJ. Ozone: its bactericidal, physiologic and deodorizing action. J Am Med Assoc 1913; 61:1008–1012.
8. Kimbell JS, Godo MN, Gross EA, et al. Computer simulation of inspiratory airflow in all regions of the F344 rat nasal passages. Toxicol Appl Pharmacol 1997a; 145:388–398.
9. Kimbell JS, Gross EA, Joyner DR, et al. Application of computational fluid dynamics to regional dosimetry of inhaled chemicals in the upper respiratory tract of the rat. Toxicol Appl Pharmacol 1993a; 121:253–263.
10. Dahl AR. Contemporary issues in toxicology: Dose concepts for inhaled vapors and gases. Toxicol Appl Pharmacol 1990; 103:185–197.

11. Miller FJ, Kimbell JS. Regional dosimetry of inhaled reactive gases. In: Henderson R, McClellan RO, eds. Concepts in Inhalation Toxicology, 2nd ed. Washington, DC: Taylor and Francis, 1995:257–287.
12. Ultman JS. Dosimetry modeling: Approaches and issues. Inhal Toxicol 1994; 6(suppl):59–71.
13. U.S. Environmental Protection Agency. Methods for Derivation of Inhaled Reference Concentrations and Application of Inhalation Dosimetry. Office of Research and Development, Washington, DC. EPA/600/8–90-066F, October, 1994.
14. Cussler EL. Diffusion: Mass Transfer in Fluid Systems, 2nd ed. New York, NY: Cambridge University Press, 1999:580.
15. Haggard HW. The absorption, distribution and elimination of ethyl ether. V. The importance of the volume of breathing during the induction and termination of anesthesia. J Biol Chem 1924; 59:795–802.
16. Morgan KT, Monticello TM. Airflow, gas deposition, and lesion distribution in the nasal passages. Environ Health Perspect 1990; 85:209–218.
17. Morris JB, Frederick CB. Upper respiratory tract uptake of acrylate ester and acid vapors. Inhal Toxicol 1995; 7:557–574.
18. Dalhamn T, Sjoholm J. Studies on SO2, NO2 and NH3: effect on ciliary activity in rabbit trachea of single in vitro exposure and resorption in rabbit nasal cavity. Acta Physiol Scand 1963; 58:287–291.
19. Miller FJ, McNeal CA, Kirtz JM, et al. Nasopharyngeal removal of ozone in rabbits and guinea pigs. Toxicology 1979; 14:273–281.
20. Frank NR, Yoder RE, Brain JD, et al. SO2 (35S labeled) absorption by the nose and mouth under conditions of varying concentration and flow. Arch Environ Health 1969; 18: 315–322.
21. Morris JB, Symanowicz PT, Olsen JE, et al. Immediate sensory-nerve mediated respiratory responses to irritants in healthy and allergic airway diseased mice. J Appl Physiol 2003; 94:1563–1571.
22. Morris JB, Clay RJ, Cavanagh DG. Species differences in upper respiratory tract deposition of acetone and ethanol vapors. Fundam Appl Toxicol 1986; 7:671–680.
23. Morris JB. Uptake of styrene vapor in the upper respiratory tracts of the CD mouse and Sprague-Dawley rat. Toxicol Sci 1999; 54:222–228.
24. Bogdanffy MS, Manning LA, Sarangapani R. High-affinity nasal extraction of vinyl acetate vapor is carboxylesterase dependent. Inhal Toxicol 1999; 11:927–941.
25. Struve MF, Wong VA, Marshall MW, et al. Nasal uptake of inhaled acrolein in rats. Inhal Toxicol 2008; 20(3):217–225.
26. Morris JB, Banton M, Pottenger LH. Uptake of inspired propylene oxide in the upper respiratory tract of the F344 rat. Toxicol Sci 2005; 81:216–224.
27. Morris JB, Pottenger LH. Nasal NPSH depletion and propylene oxide uptake in the upper respiratory tract of the mouse. Toxicol Sci 2006; 92:228–234.
28. Kimbell JS, Subramaniam RP, Gross EA, et al. Dosimetry modeling of inhaled formaldehyde: Comparisons of local flux predictions in the rat, monkey, and human nasal passages. Toxicol Sci 2001a; 64:100–110.
29. Kimbell JS, Overton JH, Subramaniam RP, et al. Dosimetry modeling of inhaled formaldehyde: Binning nasal flux predictions for quantitative risk assessment. Toxicol Sci 2001b; 64:111–121.
30. Miller FJ, McNeal CA, Kirtz JM et al. Nasopharyngeal removal of ozone in rabbits and guinea pigs. Toxicol 1979; 14:273–281.
31. Stott MJ, McKenna MJ. The comparative absorption and excretion of chemical vapors by the upper, lower and intact respiratory tract of rats. Fundam Appl Toxicol 1984; 4:594–602.
32. Casanova M, Deyo DF, Heck Hd'A. Covalent binding of inhaled formaldehyde to DNA in the nasal mucosa of Fischer 344 rats: Analysis of formaldehyde and DNA by high-performance liquid chromatography and provisional pharmacokinetic interpretation. Fundam Appl Toxicol 1989; 12:397–417.

33. Casanova M, Morgan KT, Steinhagen WH, et al. Covalent binding of inhaled formaldehyde to DNA in the respiratory tract of rhesus monkeys: Pharmacokinetics, rat-to-monkey interspecies scaling, and extrapolation to man. Fundam Appl Toxicol 1991; 17:409–428.
34. Casanova M, Morgan KT, Gross EA, et al. DNA-protein cross-links and cell replication at specific sites in the nose of F344 rats exposed subchronically to formaldehyde. Fundam Appl Toxicol 1994; 23:525–536.
35. Conolly RB, Kimbell JS, Janszen DB, et al. Human respiratory tract cancer risks of inhaled formaldehyde: Dose-response predictions derived from biologically-motivated computational modeling of a combined rodent and human dataset. Toxicol Sci 2004; 82(1):279–296.
36. Conolly RB, Lilly PD, Kimbell JS. Simulation modeling of the tissue disposition of formaldehyde to predict nasal DNA-protein cross-links in F344 rats, rhesus monkeys, and humans. Environ Health Perspect 2000; 108(suppl 5):919–924.
37. Morris JB, Hassett DN, Blanchard KT. A physiologically based pharmacokinetic model for nasal uptake and metabolism of non-reactive vapors. Toxicol Appl Pharmacol 1993; 123:120–129.
38. Frederick CB, Bush ML, Lomax LG, et al. Application of a hybrid computational fluid dynamics and physiologically-based inhalation model for interspecies dosimetry extrapolation of acidic vapors in the upper airways. Toxicol Appl Pharmacol 1998; 152:211–231.
39. Frederick CB, Lomax LG, Black KA, et al. Use of a hybrid computational fluid dynamics and physiologically-based inhalation model for interspecies dosimetry comparisons of ester vapors. Toxicol Appl Pharmacol 2002; 183:23–40.
40. Morgan KT, Jiang XZ, Starr TB, et al. More precise localization of nasal tumors associated with chronic exposure of F-344 rats to formaldehyde gas. Toxicol Appl Pharmacol 1986; 82:264–271.
41. Morgan KT, Kimbell JS, Monticello TM, et al. Studies of inspiratory airflow patterns in the nasal passages of the F-344 rat and rhesus monkey using nasal molds: Relevance to formaldehyde toxicity. Toxicol Appl Pharmacol 1991; 110:223–240.
42. Garcia GJM, Bailie N, Martins DA, et al. Atrophic rhinitis: a CFD study of air conditioning in the nasal cavity. J Appl Physiol 2007; 103:1082–1092.
43. Garcia GJ M, Schroeter JD, Segal RA, et al. Dosimetry of nasal uptake of soluble and reactive gases: A first study of inter-human variability. Inhal Toxicol 2009a; 21:607–618.
44. Kepler GM, Richardson RB, Morgan KT, et al. Computer simulation of inspiratory nasal airflow and inhaled gas uptake in a rhesus monkey. Toxicol Appl Pharmacol 1998; 150:1–11.
45. Subramaniam RP, Richardson RB, Morgan KT, et al. Computational fluid dynamics simulations of inspiratory airflow in the human nose and nasopharynx. Inhal Toxicol 1998; 10:91–120.
46. Segal RA, Kepler GM, Kimbell JS. Effects of differences in nasal anatomy on airflow distribution: A comparison of four individuals at rest. Ann Biomed Engr 2008; 36(11):1870–1882.
47. Hotchkiss JA, Herrera LK, Harkema JR, et al. Regional differences in ozone-induced nasal epithelial cell proliferation in F344 rats: Comparison with computational mass flux predictions of ozone dosimetry." Inhal Toxicol 1994; 6(suppl):390–392.
48. Kimbell JS, Morgan KT, Hatch GE, et al. Regional nasal uptake and toxicity of ozone: Computational mass flux predictions, 18O-ozone analysis, and cell replication. Toxicologist 1993b; 13:259.
49. Cohen Hubal EA, Kimbell JS, Fedkiw PS. Incorporation of nasal-lining mass-transfer resistance into a CFD model for prediction of ozone dosimetry in the upper respiratory tract. Inhal Toxicol 1996; 8:831–857.
50. Georgieva AV, Kimbell JS, Schlosser PM. A distributed-parameter model for formaldehyde uptake and disposition in the rat nasal lining. Inhal Toxicol 2003; 15:1435–1463.

51. Kimbell JS, Gross EA, Richardson RB, et al. Correlation of regional formaldehyde flux predictions with the distribution of formaldehyde-induced squamous metaplasia in F344 rat nasal passages. Mut Res 1997b; 380:143–154.
52. Monticello TM, Swenberg JA, Gross EA, et al. Correlation of regional and nonlinear formaldehyde-induced nasal cancer with proliferating populations of cells. Cancer Res 1996; 56:1012–1022.
53. Moulin FJ, Brenneman KA, Kimbell JS, et al. Predicted regional flux of hydrogen sulfide correlates with distribution of nasal olfactory lesions in rats. Toxicol Sci 2002; 66:7–15.
54. Schroeter JD, Kimbell JS, Andersen ME, et al. Use of a pharmacokinetic-driven computational fluid dynamics model to predict nasal extraction of hydrogen sulfide in rats and humans. Toxicol Sci 2006a; 94(2):359–367.
55. Schroeter JD, Kimbell JS, Bonner AM, et al. Incorporation of tissue reaction kinetics in a computational fluid dynamics model for nasal extraction of inhaled hydrogen sulfide in rats. Toxicol Sci 2006b; 90(1):198–207.
56. Schroeter JD, Kimbell JS, Gross EA, et al. Application of physiological computational fluid dynamics models to predict interspecies nasal dosimetry of inhaled acrolein. Inhal Toxicol 2008; 20(3):227–243.
57. Conolly RB, Kimbell JS, Janszen DB, et al. Dose-response for formaldehyde-induced cytotoxicity in the human respiratory tract. Regul Toxicol Pharmacol 2002; 35: 32–43.
58. Conolly RB, Kimbell JS, Janszen DB, et al. Biologically motivated computational modeling of formaldehyde carcinogenicity in the F344 rat. Toxicol Sci 2003; 75:432–447.
59. Overton JH, Kimbell JS, Miller FJ. Dosimetry modeling of inhaled formaldehyde: The human respiratory tract. Toxicol Sci 2001; 64:122–134.
60. Schlosser PM, Lilly PD, Conolly RB, et al. Benchmark dose risk assessment for formaldehyde using airflow modeling and a single-compartment DNA-protein cross-link dosimetry model to estimate human equivalent doses. Risk Anal 2003; 23:473–487.
61. Andersen ME, Sarangapani R, Frederick CB, et al. Dosimetric adjustment factors for methyl methacrylate derived from a steady-state analysis of a physiologically based clearance-extraction model. Inhal Toxicol 1999; 11:899–926.
62. Frederick CB, Gentry PR, Bush ML, et al. A hybrid computational fluid dynamics and physiologically based pharmacokinetic model for comparison of predicted tissue concentrations of acrylic acid and other vapors in the rat and human nasal cavities following inhalation exposure. Inhal Toxicol 2001; 13:359–376.
63. Csanady GA, Filser JG. A physiological toxicokinetic model for inhaled propylene oxide in rat and human with special emphasis on the nose. Toxicol Sci 2007; 95: 37–62.
64. Saragapani R, Teeguarden JG, Cruzan G, et al. Physiologically based pharmacokinetic modeling of styrene and styrene oxide respiratory-tract dosimetry in rodents and humans. Inhal Toxicol 2002; 14:789–834.
65. Teeguarden JG, Bogdanffy MS, Covington TR, et al. A PBPK model for evaluating the impact of aldehyde dehydrogenase polymorphisms on comparative rat and human nasal tissue acetaldehyde dosimetry. Inhal Toxicol 2007; 20:375–390.
66. Hinderliter PM, Thrall KD, Corley RA, et al. Validation of human physiologically based pharmacokinetic model for vinyl acetate against human nasal dosimetry data. Toxicol Sci 2005; 85:460–467.
67. Cohen Hubal, EA, Schlosser PM, Conolly RB, et al. Comparison of inhaled formaldehyde dosimetry predictions with DNA-protein cross-link measurements in the rat nasal passages. Toxicol Appl Pharmacol 1997; 143:47–55.
68. Cheng YS, Irshad H, Kuehl P, et al. Lung Deposition of Droplet Aerosols in Monkeys. Inhal Toxicol 2008; 20:1029–1036.
69. Chen BT, Weber RE, Yeh HC, et al. Deposition of cigarette smoke particles in the rat. Fundam Appl Toxicol 1989; 13:429–438

70. Wolff RK, Kanapilly GM, Gray RH, et al. Deposition and retention of inhaled aggregate $^{67}Ga_2O_3$ particles in Beagle dogs, Fischer-344 rats, and CD-1 mice Am Ind Hyg Assoc J 1984; 45(6):377–381
71. Dahlbäck M, Eirefelt S. Total deposition of fluorescent monodisperse particles in rats. Ann Occup Hyg 1994; 38(suppl 1):127–134.
72. Dohlbacket al. 1989.
73. Raabe OG, Al-Bayati MA, Teague SV, et al. Regional deposition of inhaled monodisperse coarse and fine aerosol particles in small laboratory animals. Ann Occup Hyg 1988; 32(suppl):53–63.
74. Raabe OG, HS Yeh, GJ Newton, et al. Deposition of Inhaled monodisperse aerosols in small rodents in *Inhaled Particles IV* (eds. WH Walton and B McGovern) NY: Pergamon Press, 1977:3–20.
75. Asgharian B, Kelly JT, Rewksbury EW. Respiratory deposition and inhalability of monodisperse aerosols in Long-Evans rats. Toxicol Sci 2003; 71:104–111.
76. Brenneman KA, Wong BA, Buccellato MA, et al. Direct Olfactory Transport of Inhaled Manganese ($^{54}MnCl_2$) to the Rat Brain: Toxicokinetic Investigations in a Unilateral Nasal Occlusion Model. Toxicol Appl Pharmacol 2000; 169:238–248.
77. Oberdoerster G, Sharp Z, Atudorei V, et al. Translocation of inhaled ultrafine particles to the brain. Inhal Toxicol 2004; 16:437–445.
78. Gerde P, Cheng YS, Medinsky MA. In vivo deposition of ultrafine aerosols in the nasal airways of the rat. Fundam Appl Toxicol 1991; 16:330–336.
79. Cheng YS, GK Hansen, YF Su, et al. Deposition of ultrafine aerosols in rat nasal molds. Toxicol Appl Pharmacol 1990; 106:222–233,376
80. Kelly JT, Bobbitt CM, Asgharian B. In vivo measurement of fine and coarse aerosol deposition in the nasal airways of female Long-Evans rats. Toxicol Sci 2001a; 64:253–258.
81. Kelly JT, Asgharian B, Wong BA. Inertial particle deposition in a monkey nasal mold compared with that in human nasal replicas. Inhal Toxicol 2005; 17:823–830.
82. Kelly JT, Kimbell JS, Asgharian B. Deposition of fine and coarse aerosols in a rat nasal mold. Inhal Toxicol 2001b; 13:577–588.
83. Kelly JT, Asgharian B. Nasal molds as predictors of fine and coarse particle deposition in rat nasal airways. Inhal Toxicol 2003; 15:859–877.
84. Asgharian B, Price OT, Wong BA, et al. Model of nanoparticle transport and deposition in the nasal and lung airways of humans and rats. Toxicologist, 2008; 62:204.
85. Wong B, Tewksbury AW, Asgharian B. Nanoparticle deposition efficiency in rat and human nasal replicas. Toxicologist. 2008; 62:310.
86. Rudolf G, Kobrich R, Stahlhofen W, et al. In proceedings, 7th International Symposium on Inhaled particles, September 16–20, 1991, Edinburgh, Scotland.
87. Zhang L and Yu CP. Empirical equations for nasal deposition of inhaled particles in small laboratory animals and humans. Aerosol Sci Technol 1993; 19:51–56.
88. Garcia GJM, Kimbell JS. Deposition of inhaled nanoparticles in the rat nasal passages: Dose to the olfactory region. Inhal Toxicol, 2009; 21:1165–1175.
89. Dahl AR. Snipes MB, Gerde P. Sites for uptake of inhaled vapors in beagle dogs. Toxicol Appl Pharmacol 1991; 109:263–275.
90. Dahlbäck M, Eirefelt S, Karlbergm I-B, et al. Total deposition of evans blue in aerosol exposed rats and guinea pigs. J Aerosol Sci 1989; 20(8):1325–1327.
91. Morris JB, Clay RJ, Cavanagh DG. Species differences in upper respiratory tract deposition of acetone and ethanol vapors. Fundam Appl Toxicol 1986; 7:671–680.
92. Morris JB, Cavanagh DG. Metabolism and deposition of propanol and acetone vapors in the upper respiratory tract of the hamster. Fundam Appl Toxicol 1987; 9:34–40.
93. Morris JB. First-pass metabolism of inspired ethyl acetate in the upper respiratory tracts of the F344 rat and syrian hamster. Toxicol Appl Pharmacol 1990; 102: 331–345.
94. Morris JB. Deposition of acetone vapor in the upper respiratory tract of the B6C3F1 mouse. Toxicol Lett 1991; 56:187–196.

95. Morris JB. Upper respiratory tract metabolism of inspired alcohol dehydrogenase and mixed function oxidase substrate vapors under defined airflow conditions. Inhal Toxicol 1993; 5:203–221.
96. Morris JB. Uptake of acrolein in the upper respiratory tract of the F344 rat. Inhal Toxicol 1996; 8:387–403.
97. Morris JB. Uptake of acetaldehyde and aldehyde dehydrogenase levels in the upper respiratory tracts of the mouse, rat, hamster and guinea pig. Fundam Appl Toxicol 1997; 35:91–100.
98. Morris JB, Stanek J, Gianutsos G. Sensory nerve-mediated immediate nasal responses to inspired acrolein. J Appl Physiol 1999; 87:1877–1886.
99. Morris JB. Uptake of styrene vapor in the upper respiratory tracts of the CD mouse and Sprague-Dawley rat. Toxicol Sci 1999; 54:222–228.
100. Morris JB, Wilkie WS, Shusterman DJ. Acute respiratory responses of the mouse to chlorine. Toxicol Sci 2005; 83:380–387.
101. Schlesinger RB. Comparative deposition of inhaled aerosols in experimental animals and humans: a review. J Toxicol Environ Health 1985; 15:197–214.
102. Schreider JP. Nasal airway anatomy and ihalation deposition in experimental animals and people. In: Reznik G, Stinson SF, eds. Nasal Tumors in Animals and Man, Vol. III. Boca Raton FL: CRC Press, 1983:1–26.
103. Wanner A, Mendes ES, Atkins ND. A simplified noninvasive method to measure airway blood flow in humans. J Appl Physiol 2006; 100:1674–1678.